Research Article | Vol. 29, No. 11 / 24 May 2021 / Optics Express 16893
Optics EXPRESS

Wide range thermal and athermal operation of slotted surface grating lasers

DOVYDAS MICKUS,* ROBERT MCKENNA, CAOLAN MURPHY, AND JOHN F. DONEGAN

School of Physics, CRANN and CONNECT Centre, Trinity College Dublin, Dublin 2, Ireland
*mickusd@tcd.ie

Abstract: Athermalisation is a procedure in which the wavelength of a semiconductor laser remains unchanged even as the temperature is altered. This is achieved by altering the currents that flow through the laser so as to maintain the wavelength and avoid mode hops. In this study, we demonstrate that lasers operating with a large red-shift with respect to the gain peak yield the best performance in terms of the highest temperature operation and also in terms of the widest athermal operating range. In particular, a device with red detuning of approximately 25 nm yields the best results. This device is athermalised continuously (without mode hops) from 5 to 106 ^{o}C, and discontinuously to 115 ^{o}C while maintaining wavelength stability of ±0.4 GHz/0.003 nm and side mode suppression ratio of above 40 dB in most of the continuous range and above 30 dB in the discontinuous regime. Operating in this manner will enable semiconductor lasers to be used without a thermoelectric cooler in applications where the temperature changes substantially.

1. Introduction

The rapid growth of high-speed data transmission services is increasing the demand for bandwidth and continual industry innovation is needed to meet this challenge. For optical access networks, next generation passive optical networks version 2 (NG-PON2) is an ambitious International Telecommunication Union standard developed to drive such innovation. Time and Wavelength Division Multiplexing (TWDM) has been chosen for the NG-PON2 standard. A requirement for TWDM is that there is a transmitter at every customers premises. Such wide-network deployment requires reduction of transceiver costs. Currently employed Distributed Feedback and Distributed Bragg Reflector (DBR) lasers employ low order, buried gratings to achieve high reflectivity and a wide free spectral range (FSR), however these require precise electron beam lithography and complex regrowth steps to fabricate which drive yield down [1]. One solution to this problem is to use high order, surface grating lasers which require no regrowth steps. As these lasers use high order gratings, this results in larger feature size therefore inexpensive optical lithography can be used [2], however this was not possible for this work due to limitations at the foundry. Previously such devices have been shown to exhibit high output power, good side mode suppression ratio (SMSR), low threshold and high slope efficiency.

Another significant requirement is a reduction of channel spacing, which in turn requires increased wavelength stability of transmitters. This is challenging to achieve since the emission wavelength of lasers is inherently temperature sensitive, and many applications use lasers in a variable high-temperature environment such as in data centers. Currently, thermoelectric coolers (TEC) are used to maintain a stable device temperature however, their energy efficiency and tuning precision are relatively low. Furthermore, their addition increases packaging costs and reduces package lifetime. Instead, semiconductor lasers can be athermalised, making their lasing wavelength insensitive to changes in ambient temperature [3,4] by varying injection currents across laser sections [5–8], which would allow the removal of the TEC, improving overall energy efficiency. However, athermalisation may present its own issues as devices must operate at higher

#422978 https://doi.org/10.1364/OE.422978
Journal © 2021 Received 18 Feb 2021; revised 22 Apr 2021; accepted 27 Apr 2021; published 17 May 2021

Optics EXPRESS

temperatures and laser parameters such as side mode suppression ratio (SMSR) and output power may vary significantly due to changing currents, which is undesirable. Therefore, it is of interest to investigate laser performance at higher temperatures.

Taking all of the above into account, we present a simple to fabricate, high order surface grating laser. The wavelength versus temperature dependence on various laser parameters is investigated, demonstrating that a redshift of the Bragg reflectivity peak, relative to the gain spectrum peak is beneficial to achieve improved stability and performance. This result is then used to optimize the athermal tuning of one such device, demonstrating for the first time a continuous tuning range of 5 to 106 ^{o}C and a discontinuous tuning range of 5 to 115 ^{o}C. This demonstrates that all-active, multi-section lasers allow athermal temperature ranges not achieved previously by other types of devices.

2. Device structure and athermalisation theory

The devices used in these measurements are monolithic, 700 μm long, three-section all active DBR lasers, with an integrated semiconductor optical amplifier (SOA). A sketch of a sample device is shown in Fig. 1. It should be noted that this device is part of an array, that consisted of 12 distinct devices, together which covered the C-band.

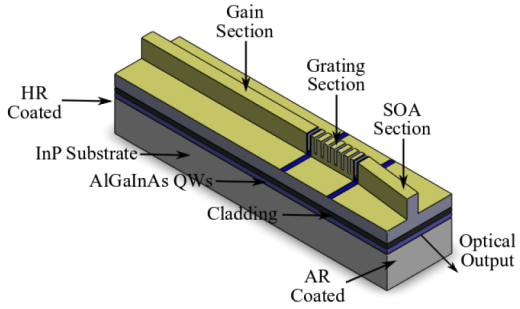

Fig. 1. An example surface grating laser. It is a multi-section device with an active grating section. Note the curved SOA. It is a sketch of a single device in a 12 device array.

They are all-active, ridge waveguide lasers, with the active medium consisting of 5 AlGaInAs quantum wells (QWs) which have the material gain peak at around 1545 nm at room temperature and with slots of the grating section etched into the 2 μm wide ridge. The lasers were fabricated on a commercially purchased wafer, which consists of 5 AlGaInAs QWs, above which there is a 1.6 μm p-doped InP layer (referred to as cladding here), 50-nm thick, p-doped InGaAsP layer, and a 200 nm InGaAs contact layer. Below the quantum wells there is 120 μm layer of InP. The slots and the ridge of the laser are fabricated using two inductively coupled plasma (ICP) etch steps using Cl_2 and N_2 gas, with the specific steps used to form the ridge/slots being the following;

1. Silicon Nitride layer is deposited using a plasma enhanced chemical vapour deposition process.
2. Electron beam lithography is used to define the slots.
3. SiO_2 is deposited to prevent etching of slots during the first ICP etch.
4. First ICP etch step is performed to a depth of 0.5 μm.
5. SiO_2 is removed to allow etching of the defined slot patterns.
6. Second ICP etch is performed to a depth of 1.35 μm. Giving slot depth of 1.35 μm.

Optics EXPRESS

The laser is subsequently contacted, cleaved and the facets are coated with high reflection (HR) and anti-reflection (AR) films, before being eutectic bonded onto an AlN carrier. As the slots were etched into the ridge, the need for regrowth steps was removed. The three sections of the ridge are the gain section, the grating section and the SOA section, with length of 470, 230 and 200 μm respectively, forming a 700 μm long laser cavity. It should be noted that the gain and grating lengths do vary slightly depending on desired lasing wavelength. The gain is used to control the gain of the material and phase, the grating is used to control the position of the Bragg peak and the SOA is used to control the output power. The SOA section is curved at 7^o to reduce back reflections from the front facet. This prevents the formation of an additional lasing cavity within the SOA section. Two different grating configurations were considered, which have been modelled, fabricated and characterised in previous publications [2,9–11]. The parameters of the first configuration are shown in Table 1.

The use of high-order gratings results in the presence of adjacent reflection peaks within the gain bandwidth, which compete with the desired mode [11]. Therefore, the second grating configuration is compromised of 23 slots, which is divided into three different periods to suppress the amplitude of adjacent FSR reflection peaks of the high-order grating. The parameters for this grating section are provided in Table 2. The chosen triple period devices were intended to be as close of a match in terms of lasing wavelength as possible to the single period devices, however due to some devices being damaged, this was not always possible.

Table 1. Parameters of the single period grating. Device here corresponds to the position of the device on the array.

Device	Period Order	Slot Order	Period Length (μm)	No. Slots	Wavelength (nm)
1	37	3.5	8.88	24	1537.52 nm
4	37	3.5	8.936	24	1547.21 nm
5	37	3.5	8.955	24	1550.5 nm
8	37	3.5	9.011	24	1560.2 nm
11	37	3.5	9.086	24	1573.18 nm

Table 2. Parameters of the triple period grating. Device here corresponds to the position of the device on the array.

Device	Period Order	Slot Order	Period Length (μm)	No. Slots	Wavelength (nm)
2	[35,41,47]	4.5	[8.417,9.86,11.303]	[8,8,7]	1540.63
4	[35,41,47]	4.5	[8.453, 9.902,11.351]	[8,8,7]	1547.22
6	[35,41,47]	4.5	[8.488, 9.943,11.398]	[8,8,7]	1553.62
8	[35,41,47]	4.5	[8.524, 9.985,11.446]	[8,8,7]	1560.21
10	[35,41,47]	4.5	[8.56, 10.027,11.494]	[8,8,7]	1566.8
12	[35,41,47]	4.5	[8.595, 10.068,11.542]	[8,8,7]	1573.21

Athermalisation for these devices is achieved by varying the injection currents to the gain and grating sections, with the SOA section having only a weak effect on wavelength. As these lasers are all-active, once threshold is achieved the carrier density remains almost constant. Therefore unlike devices with passive sections, tuning due to the carrier induced plasma effect plays a minor role and thermal tuning dominates [12]. Hence, for athermalisation, as ambient temperature is changed, injection currents are also varied to vary the self-heating of the device in such a way that the local device temperature remains constant while operating within a single mode. So, to achieve athermal operation over a wide range of ambient temperatures we must be able to induce

Optics EXPRESS

a large change in the self-heating, therefore the devices must be able to operate at large currents at low ambient temperatures and by proxy, must be able to operate at large local temperatures. Therefore, the next section will investigate the thermal performance of our lasers in order to find a candidate that is capable of operating at high ambient temperature.

3. Thermal tuning results

The devices were tested on a setup shown in Fig. 2. The lasers were contacted and biased at 100 mA into the gain and grating sections. The SOA section was provided with 30 mA of current. The output light was then coupled using a lensed fibre and passed through 90:10 splitter, where 90 percent travels to a Agilent 86140B optical spectrum analyser (OSA) which has a resolution of ±0.01 nm. The rest travels to a PIN diode which was used to optimise coupling by maximising coupled power. The temperature of the copper heatsink was monitored using a thermistor.

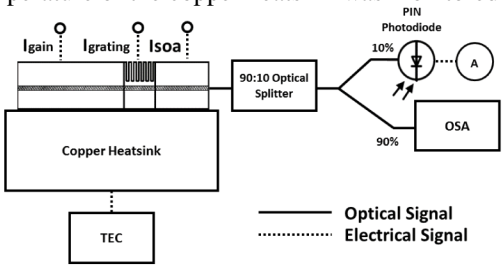

Fig. 2. Steady state characterisation setup.

A TEC was used to sweep temperatures from 20 to 100 ^{o}C in 10 ^{o}C intervals to simulate various ambient temperatures, and if FSR mode hops are approached the temperature steps are reduced to show the transition between FSR modes. The wavelength vs temperature performance of the single period array is shown in Fig. 3. It is observed that there exist abrupt changes in wavelength which correspond to FSR mode hops. This is an inherent disadvantage of high order gratings. While the occurrence such phenomena has been reported in single period arrays in detail [11], it is interesting to note that redder wavelengths clearly give a larger thermal tuning range within the intended FSR mode which has not been previously reported. For example, the bluest laser in the array does not lase within its intended FSR mode at 20 ^{o}C, however the reddest laser remains within the intended mode until 70 ^{o}C where it mode hops to the next FSR mode. As this thermal tuning range is still relatively low for large range athermalisation purposes, the single period devices are then deemed unsuitable for this application.

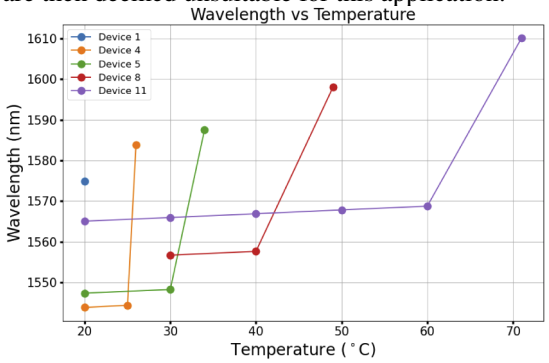

Fig. 3. Thermal tuning behaviour of individual devices on the single period array.

The wavelength versus temperature relationship for the triple period array is shown in Fig. 4.

Optics EXPRESS

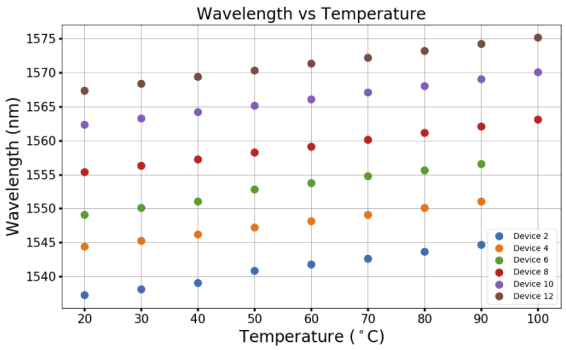

Fig. 4. Thermal tuning of our triple period laser array. It is capable of covering the entire C-band.

Clearly we can see that there are no discontinuities in wavelength and the tuning behaviour is linear with temperature. This is a result of the suppression of the adjacent FSR peaks and allows for a much larger temperature tuning range. In fact, the devices never mode hop to the adjacent FSR modes and instead fall below threshold if the temperature is too high. The observed trend is that redder wavelengths operate to higher temperatures. This is due to the misalignment of the gain spectrum peak and the Bragg reflective peak, which is referred to as detuning. This has been demonstrated before in [13], however the impact of detuning on SMSR was not shown and hence is investigated here in Fig. 5. Measurements recorded the SMSR of the peaks within the intended reflective peak (local SMSR) range, which was done using a short span and also recorded the overall SMSR (global) using a wide span on the OSA. This was done because the global SMSR also includes lasing peaks from the next FSR while the local SMSR does not. This difference in SMSR is here defined as the SMSR penalty. The effect of the next FSR modes on SMSR is typically significant while using high-order gratings due to a low FSR and hence, the impact of this is important to investigate. As seen in Fig. 5, local SMSR is observed to be very high at ambient temperatures and decreases with increasing temperature. However, local SMSR of bluer lasers is observed to be lower, as seen in Fig. 5(d) and it also decreases more rapidly than lasers with more red-shifted emission, with the change of SMSR over the thermal tuning range being plotted as SMSR loss (see Fig. 5(e)). Average wavelength here designates the central wavelength within the tuning range. This variance in SMSR is due to the gain spectrum redshifting with increased ambient temperature, providing more gain to red wavelengths with increasing temperature. This is shown as increased stability of the SMSR for red lasers, with the highest stability observed at around +(20-25) nm away from the material gain peak. Past this point the benefits of detuning appear to diminish. Furthermore, when observing the global SMSR, it can be seen that blue end lasers experience a significant amount of mode competition from the next FSR. This is not the case for lasers past approximately 1555 nm as seen in Fig. 5(f). Additionally, the effect on output power versus detuning was also investigated, which is a first for simple, ridge waveguide lasers operating within the C-band. Looking at the output power data in Fig. 6, there is a typical relationship of decreasing power with temperature, with the total loss in power over the tuning range plotted in 6(c). This is due to increase in leakage current and non-radiative recombination at higher ambient temperatures. However, it can be seen that redder emitting devices maintain their output power more steadily(see Fig. 6(c)). It should be noted that both Fig. 5(e) and 6(c) consider only the changes of the power/SMSR of the devices from 20 to 90 ^{o}C as blue-end devices (number 2,4 and 6) went below threshold at 100 ^{o}C. It can be clearly seen that the general trend suggests redder wavelengths lose less power when temperature is increased, however the benefit of additional detuning seems to diminish. This suggests that past a

Optics EXPRESS

certain point there is no additional benefit in detuning the laser further, which seems to be around 25 nm, which can be contrasted with a similar result derived for Mid-IR lasers in Ref. [14]. In the lasers studied in this reference, there is a benefit to have a detuning of up to +250 nm.

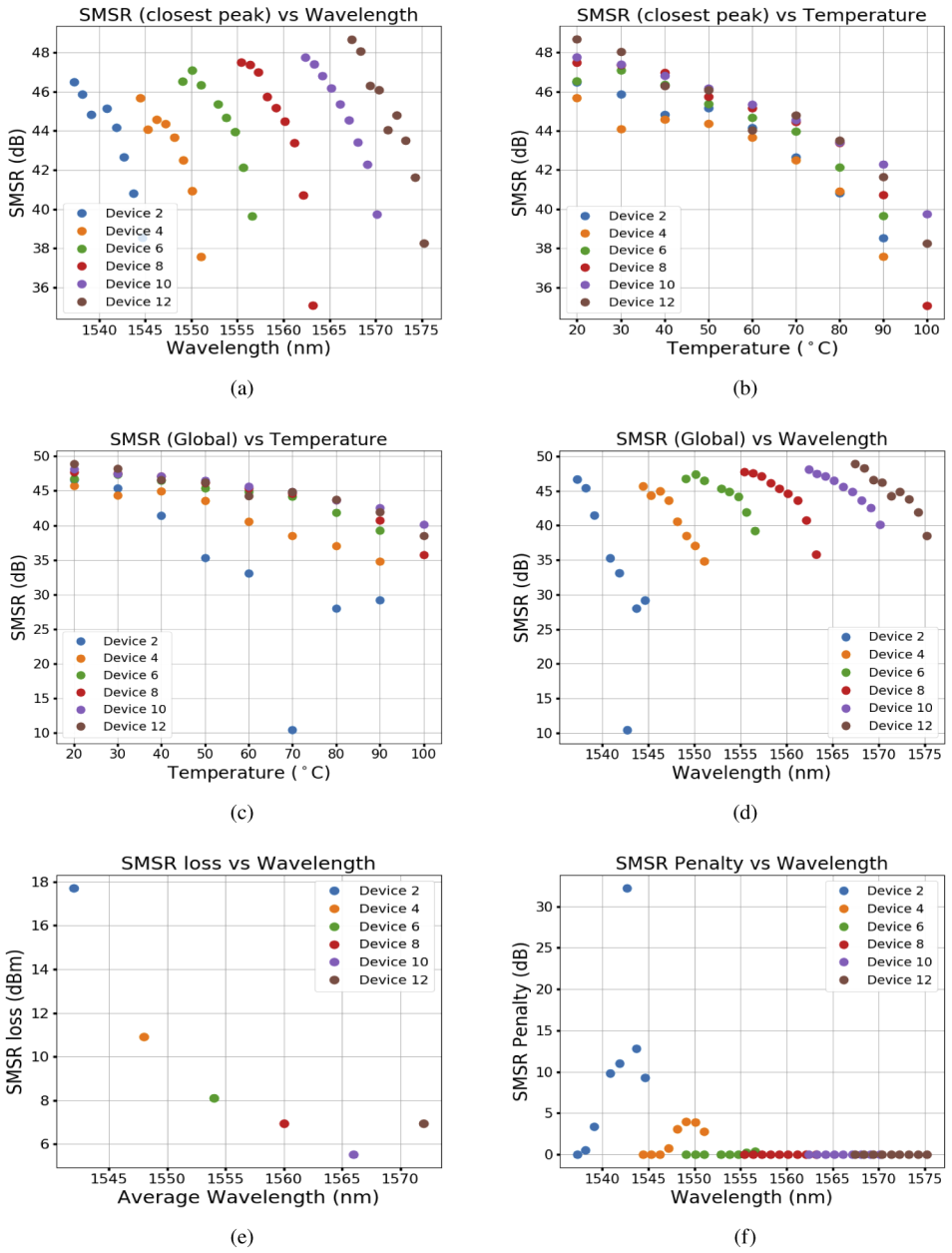

Fig. 5. (a) SMSR of the closest peak vs Wavelength (b) SMSR of the closest peak vs Temperature (c) Global SMSR vs Wavelength (d) Global SMSR vs Temperature (e) SMSR loss vs Average Wavelength over tuning range (f) SMSR Penalty vs Wavelength. All for triple period grating devices.

Optics EXPRESS

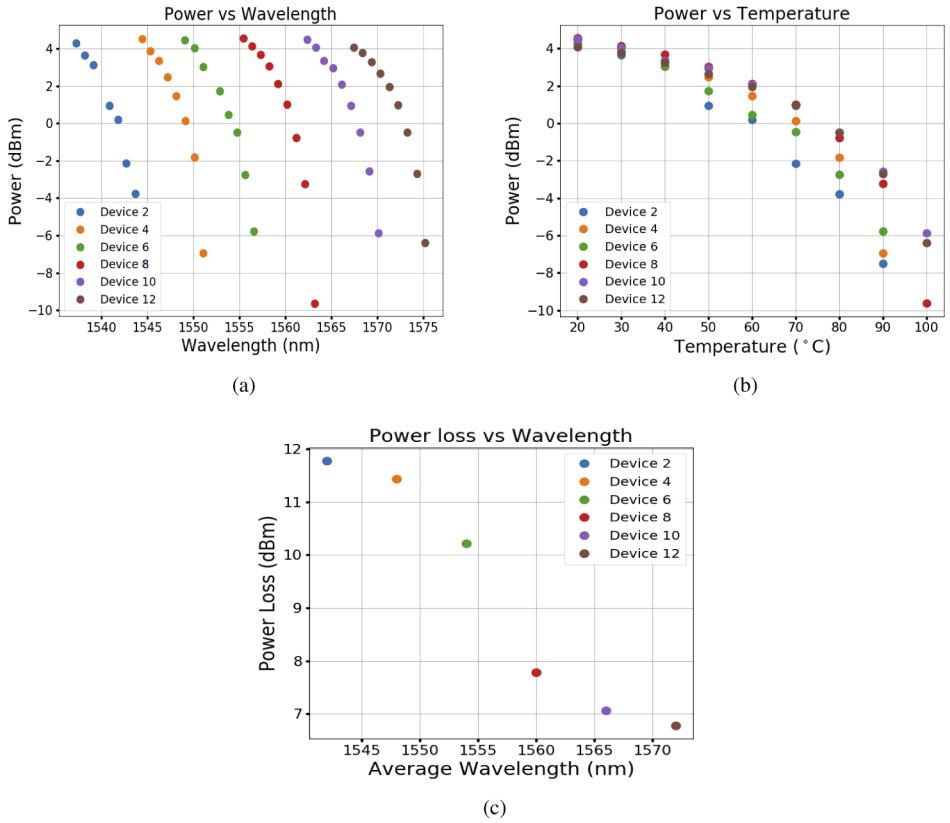

Fig. 6. (a) Power vs Wavelength (b) Power vs Temperature (c) Loss in Power over the thermal tuning range vs Average Wavelength. All for triple period grating devices.

4. Athermalisation results

Since the results of the previous section suggest that devices with redder wavelengths behave more favourably at elevated temperatures, we chose a device on the red end of the laser array for our athermalisation studies. A tuning map of our laser taken at 20 ^{o}C is presented in Fig. 7 with the currents used for athermalisation plotted in black.

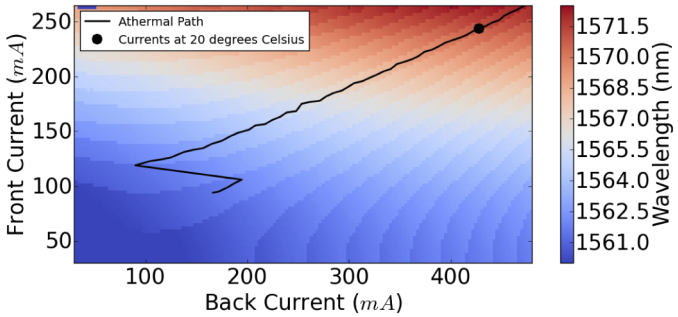

Fig. 7. Tuning map of our device taken at 20 ^{o}C. The black line denotes the athermal path, and the black point shows corresponding currents at 20 ^{o}C.

Optics EXPRESS

As can be seen, at very low currents(<100 mA in each section) the free carrier plasma effect tuning is present, however at any reasonable current the thermal tuning is dominant. One important thing to note is that due to this effectively being thermal tuning, the length of each section is important. Shorter sections lead to higher resistance and hence, higher input power per unit of input current, allowing shorter devices to achieve large temperature deviations more easily and therefore larger tuning ranges. Hence, lasers chosen for this athermlisation are 700 μm in length as opposed to the 1 mm from previous work [15,16], with a grating of approximately 230 μm and a gain section of 470 μm. This gain section length is still long enough to provide significant amount of gain, resulting in good output power and relatively low linewidth [1]. The athermalisation results are shown in Fig. 8. We traverse the path as shown in Fig. 7 by slowly changing the TEC temperature and adjusting the currents to the front and back sections. The wavelength is maintained to within ±0.4 GHz or 0.003 nm via precise tuning of current, which is well within the required maximum spectral excursion requirement of ±12.5 GHz or 0.4 nm for 50 GHz spaced channels on a TWDM grid [17]. This resolution is higher than the OSA used in the previous measurement, however for the measurements presented here, the wavelength was obtained from a HP 86120B wavemeter with a resolution of ±2 pm , while the SMSR was obtained using the OSA. It is seen that the SMSR was maintained above 40 dB from 5 to 102 ^{o}C, after which it remains above 30 dB, which is also within TWDM requirements. Output power for this athermalisation was measured using a bare photodiode to get the absolute power and is remains relatively stable until it reaches about 80 ^{o}C, decreasing more rapidly from that point onwards as the TEC temperature is increased. This is because as ambient temperature is increased, currents in each tuning section must be reduced to compensate for the increase in temperature, however this leads to a reduction in carriers for stimulated recombination and hence lower output power. An increase in output power is observed at 108 ^{o}C, which is due to a discontinuous mode hop. This discontinuous mode hop was necessary as the device was approaching threshold, hence an increase in gain current was provided. As no such discontinuities are observed before this point, it is clear that the tuning in the range 5 to 106 ^{o}C is continuous.

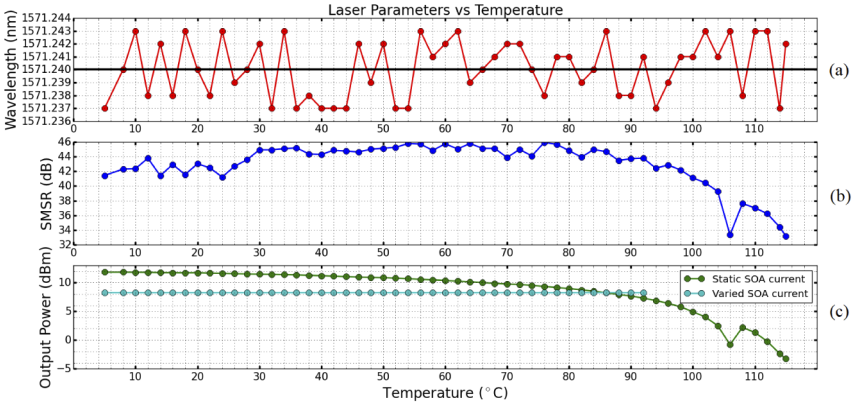

Fig. 8. (a) Wavelength vs Temperature. The black line denotes center of TWDM channel 8. (b) Wavelength vs SMSR. Note the decrease in SMSR at high ambient temperature. (c) Wavelength vs Power for both static and varied SOA currents. Note how output power can be stabalised from 5 to 94 ^{o}C.

Furthermore, output power is maintained above 0 dBm in all but the last point in the continuous range. This output power variation can also be reduced to less than ±0.005 dBm by varying the SOA current as shown in Figs. 8(c) and 9. As observed in Fig. 8, the decrease in power seems to increase more drastically with increasing temperature. In turn, this will cause a sharper rise in SOA current at higher temperatures and will lead to the SOA saturating relatively quickly, which

Optics EXPRESS

occurs at ≈60 mA which is the SOA current at 92 ^{o}C. Past this point the loss in output power is too large and was not compensated. One possible solution to stabilising power within the entire range is to redesign the SOA, such as increasing the length of the SOA section so it can provide a larger amount of gain over a larger temperature range, however this was not performed for this study.

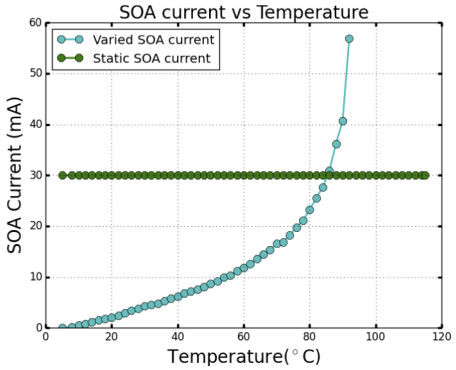

Fig. 9. SOA currents for either maintaining static power or static SOA current.

The athermalisation results shown here, in terms of the small wavelength variation and wide temperature range are the best achieved to date. They show that careful control of currents that flow to the device from monitoring temperature changes allow for very precise control on the laser wavelength. This result has the potential to influence the range of applications where these lasers operate in temperature varying environments. Currents used for the athermalisation are displayed in Fig. 10. As mentioned earlier, high currents are needed at low temperatures to achieve high self-heating and hence a wide athermal range. Additionally, only one large discontinuity in current is observed proving that the tuning in the range of 5 to 106 ^{o}C was indeed continuous. Another measurement that was taken to further solidify this is input electrical power versus temperature which is shown in Fig. 11.

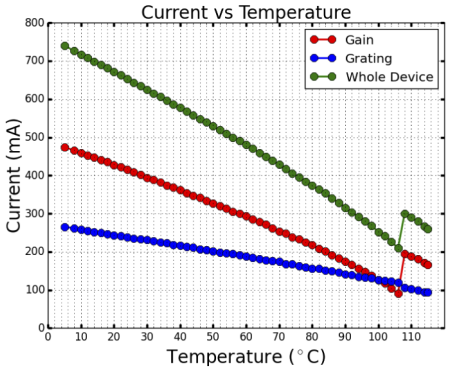

Fig. 10. Currents used to achieve athermal performance.

As discussed previously, temperature must remain constant for all-active devices within a mode during athermalisation, and so electrical input power must vary linearly to combat the changes in temperature. This linear relationship is observed in two parts within Fig. 11, suggesting that there is only two modes present during this athermalisation. For this device, the slope from Fig. 11 is observed to be −0.023 $W/^{o}$C, −0.016 $W/^{o}$C and −0.0078 $W/^{o}$C for the whole device, gain and

Optics EXPRESS

grating sections respectively. Furthermore, as the slope gives the power change needed to offset an ambient temperature change of 1 ^{o}C, then these slopes can be used to calculate the thermal resistance of each section via $Z = \frac{1}{|S|}$ where S is the slope. For the gain and grating sections respectively, these are 62.5 and 128.2 ^{o}C/W. Then, the thermal resistivity for the ridge can be obtained by multiplying by the length of the respective section giving ≈29.4 ^{o}C μm/mW.

Finally, the wall plug efficiency over the athermal range is shown in Fig. 12 and is observed to increase until approximately 80 ^{o}C, however from this point on it is observed to drop rapidly. This is because of a rapid decline in output power as a result of decreasing stimulated recombination past this point. Do note that the TEC was not included in the wall plug efficiency calculation as it was merely used to simulate various ambient temperatures. This performance is a 54 ^{o}C improvement over our previous work [15] while tuning continuously and a 20 ^{o}C improvement while tuning discontinuously, clearly demonstrating that choice of laser wavelength and length of lasing sections are important factors when designing lasers for athermalisation.

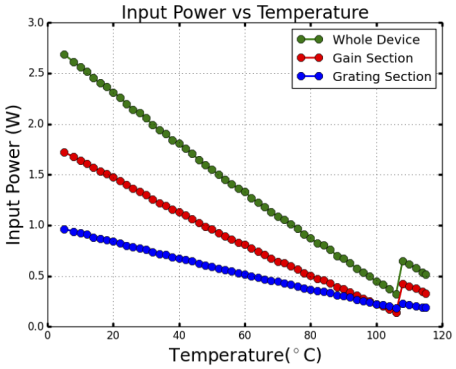

Fig. 11. Electrical input power into our laser over the athermal path.

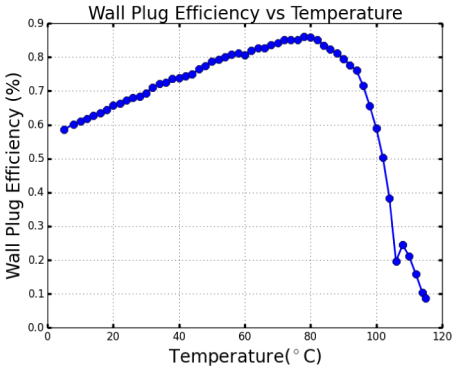

Fig. 12. Wall Plug Efficiency over our athermal path.

5. Conclusion

In conclusion, a clear relationship for Bragg peak position with respect to gain spectrum peak is established for parameters of output power and SMSR, for surface grating lasers operating in the C-band. This result indicates that when the grating wavelength is designed to be at a red end, relative to the material gain spectrum peak, improved thermal tuning performance is observed. In

Optics EXPRESS

particular, it was observed that the benefits of this detuning saturate at +25 nm from the material gain peak. This result was then used to athermalise a device continuously from 5 to 106 ^{o}C, and discontinuously to 115 ^{o}C with a wavelength variation of ±0.4 GHz/0.003 nm which is well within the TWDM specifications. Hence this work presents a promising candidate for uncooled TWDM networks and a method to improve already existing devices for temperature sensitive applications.

Funding. Science Foundation Ireland (15/IA/2854).

Disclosures. The authors declare no conflicts of interest.

References

1. A. Abdullaev, Q. Lu, W. Guo, M. J. Wallace, M. Nawrocka, F. Bello, A. Benson, J. O'Callaghan, and J. F. Donegan, "Improved performance of tunable single-mode laser array based on high-order slotted surface grating," Opt. Express **23**(9), 12072–12078 (2015).
2. Q. Lu, W.-H. Guo, D. Byrne, and J. F. Donegan, "Design of Slotted Single-Mode Lasers Suitable for Photonic Integration," IEEE Photonics Technol. Lett. **22**(11), 787–789 (2010).
3. B. R. Koch, E. J. Norberg, B. Kim, J. Hutchinson, J.-H. Shin, G. Fish, and A. Fang, "Integrated Silicon Photonic Laser Sources for Telecom and Datacom," in *2013 Optical Fiber Communication Conference and Exposition and the National Fiber Optic Engineers Conference (OFC/NFOEC)*, (2013), pp. 1–3.
4. J. Bovington, S. Srinivasan, and J. E. Bowers, "Athermal laser design," Opt. Express **22**(16), 19357–19364 (2014).
5. S. H. Lee, A. Wonfor, R. V. Penty, I. H. White, G. Busico, R. Cush, and M. Wale, "Self-configuring athermal tunable DS-DBR laser for passive optical networks," in *CLEO/QELS: 2010 Laser Science to Photonic Applications*, (2010), pp. 1–2.
6. J. Zhu, A. Wonfor, S. H. Lee, S. Pachnicke, M. Lawin, R. V. Penty, J.-P. Elbers, R. Cush, M. J. Wale, and I. H. White, "Athermal Colorless C-Band Optical Transmitter System for Passive Optical Networks," J. Lightwave Technol. **32**(22), 4253–4260 (2014).
7. M. Roppelt, M. Roppelt, F. Pohl, K. Grobe, M. Eiselt, and J.-P. Elbers, "Tuning Methods for Uncooled Low-Cost Tunable Lasers in WDM-PON," in *Optical Fiber Communication Conference/National Fiber Optic Engineers Conference 2011 (2011), paper NTuB1*, (Optical Society of America, 2011), p. NTuB1.
8. Y. Liu, A. Davies, J. Ingham, R. Penty, and I. White, "Uncooled DBR laser directly Modulated at 3.125 gb/s as athermal transmitter for low-cost WDM systems," IEEE Photonics Technol. Lett. **17**(10), 2026–2028 (2005).
9. F. Bello, A. Abdullaev, M. Wallace, M. Nawrocka, Q. Lu, W. Guo, and J. F. Donegan, "Traveling Wave Analysis for a High-Order Grating, Partially Slotted Laser," IEEE J. Quantum Electron. **51**(11), 1–5 (2015).
10. Q. Y. Lu, W. H. Guo, R. Phelan, D. Byrne, J. F. Donegan, P. Lambkin, and B. Corbett, "Analysis of Slot Characteristics in Slotted Single-Mode Semiconductor Lasers Using the 2-D Scattering Matrix Method," IEEE Photonics Technol. Lett. **18**(24), 2605–2607 (2006).
11. G. Jain, M. J. Wallace, R. McKenna, K. Brazel, F. Bello, Q. Lu, W. Guo, and J. F. Donegan, "Design Optimization for Semiconductor Lasers With High-Order Surface Gratings Having Multiple Periods," J. Lightwave Technol. **36**(22), 5121–5129 (2018).
12. R. McKenna, D. Mickus, S. Naimi, C. Murphy, M. McDermott, S. Corbett, D. McCloskey, D. McCloskey, D. McCloskey, D. McCloskey, J. F. Donegan, J. F. Donegan, J. F. Donegan, and J. F. Donegan, "Spatially resolved self-heating and thermal impedance of laser diodes using CCD-TR imaging," OSA Continuum **4**(4), 1271–1281 (2021).
13. Y. Nishimoto, H. Yagi, K. Miura, D. Plumwongrot, K. Ohira, T. Maruyama, and S. Arai, "High T0 Operation of 1590 nm GaInAsP/InP Quantum-Wire Distributed Feedback Lasers by Bragg Wavelength Detuning," Jpn. J. Appl. Phys. **46**(17), L411–L413 (2007).
14. F. Xie, C. Caneau, H. P. Leblanc, S. Coleman, M.-T. Ho, C. A. Page, L. C. Hughes, and C.-E. Zah, "Impact of Wavelength Detuning on the Performance of Mid-IR Distributed Feedback Quantum Cascade Lasers," IEEE J. Sel. Top. Quantum Electron. **19**(4), 1200508 (2013).
15. D. Mickus, G. Jain, S. Naimi, R. McKenna, C. Murphy, and J. F. Donegan, "Athermal Operation of Multi-Section Surface Grating Lasers for Applications Including Burst-Mode for TWDM-PONs," in *2020 Conference on Lasers and Electro-Optics (CLEO)*, (2020), pp. 1–2. ISSN: 2160–8989.
16. M. J. Wallace, R. O. Meehan, R. Enright, F. Bello, D. McCloskey, B. Barabadi, E. N. Wang, and J. F. Donegan, "Athermal operation of multi-section slotted tunable lasers," Opt. Express **25**(13), 14414–14426 (2017).
17. ITU-T, "ITU-T Recommendation G.989.1 40-Gigabit-capable passive optical networks (NG-PON2): General requirements," Itu-T G-Series Recommendations (2013).